POLITECNICO
MILANO 1863

SCUOLA DI INGEGNERIA INDUSTRIALE
E DELL'INFORMAZIONE

Executive Summary of the Thesis

Light-induced Floquet states with few-femtosecond pulses

Laurea Magistrale in Engineering Physics - Ingegneria Fisica

Author: Matteo Talarico

Advisor: Prof. Matteo Lucchini

Co-advisor: Dr. Fabio Medeghini

Academic year: 2020-2021

1. Introduction

Floquet theory was develped by Gaston Floquet in the late 19^{th} century. This theory is vastly useful in the treatment of linear differential equations with periodic coefficients, and lends itself to the description of numerous physical phenomena which present a periodicity.
This theory can be applied in quantum mechanics if we consider the Time-Dependent Schrödinger Equation (TDSE)

$$i\hbar\frac{\partial}{\partial t}|\psi(t)\rangle = \hat{H}(t)|\psi(t)\rangle \tag{1}$$

written for a periodic Hamiltonian $\hat{H}(t)$, and with $|\psi(t)\rangle$ as the system wave-function.
Hence, its solution can be written as

$$|\psi(t)\rangle = |\phi(t)\rangle e^{-i\epsilon t}$$

with ϵ being the so-called *Floquet quasi-energy* and $|\phi(t)\rangle = |\phi(t+T)\rangle$, which thanks to its periodicity can be expanded in series as follows:

$$|\phi(t)\rangle = \sum_{n=-\infty}^{+\infty} A_n e^{-in\omega t} \tag{2}$$

The results of Eqs. (1) and (2) find application in a plethora of research areas. Solid-state physics is an example [4], where the Floquet theory is commonly used to describe the properties of matter driven by a periodic light field. Some of its applications can be found in Floquet topological insulators or in nuclear magnetic resonance spectroscopy. In particular, Floquet theory finds its value in a new branch of physics called *Floquet engineering* [4], i.e. the manipulation and control of quantum systems via periodic driving, usually of the electromagnetic kind. Laser fields are able to provide such a periodicity, for instance in the study of quantum materials [4] or of the atomic light shift.
While the Floquet formalism has been vastly used and tested with quasi-monochromatic light drivings, it is not clear if its concept can be extended to the short-pulse limit, where the light-dressed states could be employed to switch the optical properties of materials on ultrafast time scales. Indeed, due to their short duration few-cycle pulses lose their periodicity and border effects become rather relevant, and we may not be able to apply Floquet theory any longer. Hence, the objective of this thesis is to explore the limits of Floquet theory in the case of ultrashort pulses.
To pursue this goal, we performed a pump-probe spectroscopy experiment on a Ne gas target using a few-fs extreme-ultraviolet (XUV) probe

and an infrared (IR) driving pulse of variable duration between 9 and 150 fs. In the following we will indicate with τ_{XUV} and τ_{IR} their respective duration. At first, we will investigate the behaviour of the system for long IR pulses as the IR intensity varies. Afterwards, we will investigate the effect of a finite driving pulse on the induced Floquet states.

2. Methodology

2.1. Optical setup

In our optical setup (Figure 1), the main light source consists of an ultrafast Ti:Sapphire laser operating in mode-locking regime used as a seed, with a wavelength of $\lambda_{IR} = 811$ nm ($E_{IR} = 1.53$ eV) and a repetition rate of $f_{rep} = 1$ kHz. It is then amplified up to an energy of $E_{out} = 7$ mJ through a chirped-pulse amplification (CPA) stage, which employs high-power Q-switched laser as a pump.
At the laser exit, a beam splitter divides the beam into two paths. The first path ($P_{IR,1}$ = 1.2 W) leads to the generation of the XUV pulses through *High-order Harmonic Generation (HHG)* [3] and the selection of the correct frequency via a *Time Delay-Compensated Monochromator (TDCM)* [5]. The second path ($P_{IR,2}$ = 1 W) leads to the *hollow-core fibre (HCF)* compression setup, which is used to tailor the pulse duration. The two beams are collimated onto a Ne gas target inside a *Time-of-Flight spectrometer (ToF)*, where the experiment takes place. A delay stage on the second path is employed after the HCF to vary the temporal distance between the two paths.

2.2. Pump-probe experiment

To perform the experiment the TDCM is used to select the 23^{rd} harmonic of the IR beam ($E_{XUV} = 35.23$ eV, or $\lambda_{XUV} = 35.26$ nm). This beam is used to generate photoelectrons with an energy of $E_{MB} = E_{XUV} - E_{ion.,Ne} = 13.67$ eV, which we will call *main band*, MB; if an opportunely delayed IR pulse is added to the process, its field dresses the photoelectron final state inducing the formation of sideband peaks in the photoelectron spectrum. Those shall be indicated as $\mathrm{SB}^{N\pm}$, with $N \in \mathbb{Z}$ being the number of photons absorbed (+) or emitted (-), following the scheme of Figure 2.

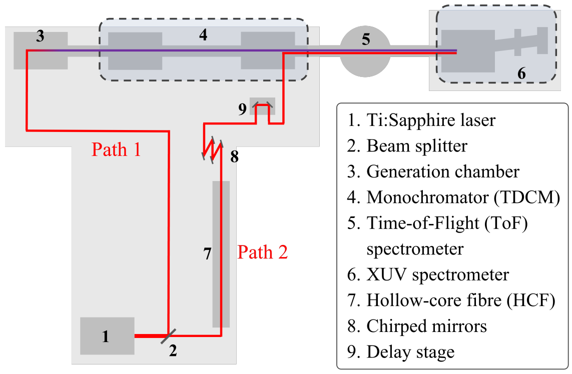

Figure 1: Simplified schematics of the optical setup and of the path travelled by the laser. In red, IR radiation ($\lambda_{IR} = 811$ nm); in purple, XUV radiation ($\lambda_{XUV} = 35.26$ nm).

The number of generated sidebands grows with the IR laser intensity. Furthermore, by increasing I_{IR} the main band becomes more depleted, accordingly to particle conservation. Actually, if we keep increasing the IR intensity with respect to the XUV one, we will reach a point in which the sidebands will start to empty too in order to fill higher order ones. More details about these phenomena are given in Section 3.

2.3. Beam characterisation

For a complete analysis of our results it is essential to know the pulse intensity and temporal characteristics.
As for the pulse characterisation, many techniques were employed. To retrieve the intensity of our IR pulses we measured their power and utilised a beam profiler to collect the spatial distribution of their energy. Spectrometers were also employed for the spectrum of both IR and XUV. The IR temporal profile was measured via *second-harmonic generation frequency-resolved optical gating*, otherwise known as *SHG-FROG*.
Another method used for pulse reconstruction is the *Simplified Trace Reconstruction In the Perturbative regimE* (**STRIPE**) [1], a reconstruction algorithm based on the Strong Field Approximation (SFA) capable of full pulse reconstruction. We will use it to reconstruct the XUV pulses. The main idea is the following: given in input the IR pulse shape, the XUV spectrum and the experimental spectrogram, a guess is made of the XUV phase; then, a new spectrogram is simulated from those values, it is con-

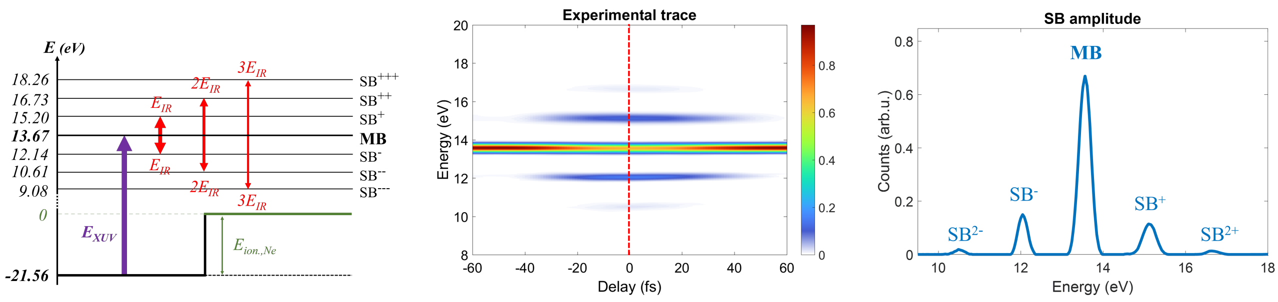

(a) (b) (c)

Figure 2: (a) Ionisation process and SB generation scheme. (b) Example of experimental spectrogram as a function of energy and time delay τ. (c) SB amplitudes as a function of energy at $\tau = 0$ fs and $I_{IR} = 6.58 \cdot 10^{11} \frac{W}{cm^2}$.

voluted with the instrumental response of the ToF spectrometer, and it is compared to the real spectrogram; based on this difference, a new guess is made for the XUV phase, and this process is iterated until the difference between the two spectrograms is close to null within a certain margin.

Before using STRIPE we had to clean the signal of the raw spectrogram trace. For each time delay we recorded a spectrogram without IR pulses and used its trace to characterise the noise of the main band, which is proportional to that of the sidebands. We employed a noise removal algorithm and a Gaussian fit to estimate the noise, and we subtracted it from each sideband to obtain a clean trace.

3. Floquet theory in the Strong Field Approximation

Strong Field Approximation, or **SFA**, is an approach that allows to describe many phenomena, and two-colour photoexcitation is one of them. In the following analysis we utilise a *semi-classical approach* in a *non-relativistic framework*; we use the *Single Active Electron (SAE)* formulation, implying the presence of exclusively one electron evolving according to the TDSE of Eq. (1); we make use of *atomic units (a.u.)*.

Starting from the Maxwell Equations and from the TDSE, and by making a few other assumptions an approximations (such as the *Dipole Approximation*) [3], it is possible to write the spectrogram as:

$$S(\omega,\tau) = \left| \int_{-\infty}^{+\infty} \mathbf{E}_{XUV}(t+\tau) e^{i\phi(\mathbf{p},t)} e^{i(\frac{1}{2}p^2+I_P)t} dt \right|^2$$

with the phase ϕ being

$$\phi(\mathbf{p},t) = -\int_t^{+\infty} \mathbf{p}\cdot\mathbf{A}_{IR}(t') + \frac{A_{IR}^2(t')}{2} dt'$$

where τ is the time delay, $\mathbf{E}_{XUV}$ is the XUV field, $\mathbf{p}$ the final electron momentum, I_P the ionisation potential, and $\mathbf{A}_{IR}$ the IR vector potential.

If we now consider $\mathbf{A}_{IR} = A_0\cos(\omega_0 t)$ and assume $A_{IR}^2 \simeq 0$, this result can be further simplified by means of the *Central Momentum Approximation (CMA)*, to find the *simplified SFA model*:

$$S(\omega,\tau) = \left| \int_{-\infty}^{+\infty} \mathbf{E}_{XUV}(t+\tau) e^{ip_C \frac{A_0}{\omega_0}\sin(\omega_0 t)} e^{i\omega t} dt \right|^2 \tag{3}$$

having $\mathbf{p}_C$ as the central momentum and ω as the frequency. We notice that we can write Eq. (3) as the Fourier transform of a periodic function

$$f(t,\tau) = \mathbf{E}_{XUV}(t+\tau) e^{ip_C \frac{A_0}{\omega_0}\sin(\omega_0 t)}$$

which can be expanded in Fourier series, to obtain a result akin to Eq. (2) [2].

3.1. Frequency (Bessel) expansion

To expand $f(t,\tau)$ in series we can make use of the *Jacobi-Anger expansion*:

$$e^{iz\sin(\vartheta)} = \sum_{n=-\infty}^{+\infty} J_n(z) e^{in\vartheta}$$

where J_n are the *Bessel functions of the first kind* of order n, and considering $z = p_C \frac{A_0}{\omega_0}$ and $\vartheta = \omega_0 t$.

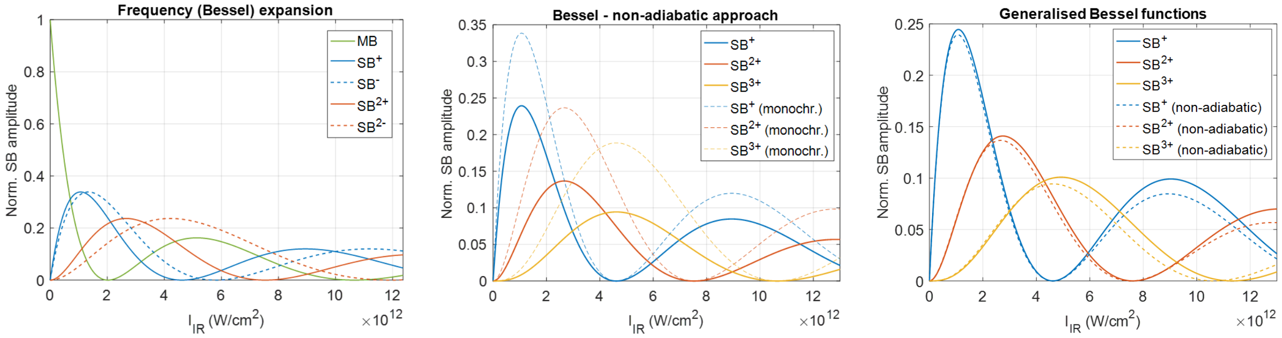

(a) (b) (c)

Figure 3: Amplitude of MB and SB as a function of the IR intensity at $\tau = 0$ In case of (a) Bessel expansion, (b) non-adiabatic approximation, compared to the simple Bessel expansion in the case $\tau_{IR} = \tau_{XUV} = 11$ fs, and (c) generalised Bessel function model compared to non-adiabatic model for $\tau_{IR} = \tau_{XUV} = 11$ fs.

Therefore, if we consider that the XUV field is oscillating at a frequency ω_x with an amplitude E_x, we can write the spectrogram of Eq. (3) as

$$S(\omega,\tau) = \left| \mathcal{F}\left[E_x \sum_{n=-\infty}^{+\infty} J_n\left(-p_C\frac{A_0}{\omega_0}\right) e^{-i(\omega_x+n\omega_0)t} \right] \right|^2$$

If we now normalise with respect to the XUV field and we consider the SB amplitude as a function of I_{IR}, we find that each amplitude is represented by the square modulus of a Bessel function in which the SB order corresponds to the order n of the function (Figure 3a).

3.2. Non-adiabatic approach

In the previous section we assumed A_0 to be constant. Now we shall consider fields that are dependent on time. In particular, we choose the IR and XUV pulses to be Gaussian, so to have $A_0(t) = \frac{E_0}{\omega_0} e^{-\frac{t^2}{\tau_{IR}^2}}$ and $E_{XUV}(t+\tau) = E_x e^{-\frac{(t+\tau)^2}{\tau_{XUV}^2}}$.

Then, from numerical computations we observe that if the pulse envelope evolves on a longer time scale than its oscillation cycle (*Slowly-Varying Envelope Approximation*, or *SVEA*), we can approximate the Bessel functions as

$$J_N\left(-p_C\frac{E_0}{\omega_0^2}e^{-\frac{t^2}{\tau_{IR}^2}}\right) \simeq J_N\left(-p_C\frac{E_0}{\omega_0^2}\right) e^{-|N|\frac{t^2}{\tau_{IR}^2}} \tag{4}$$

leading $\mathrm{SB}^{N\pm}$ to have a maximum value equal to

$$SB_0^{N\pm} \simeq \left| J_N\left(-p_C\frac{E_0}{\omega_0^2}\right)\right|^2 \frac{1}{\sqrt{1+|N|\frac{\tau_{XUV}^2}{\tau_{IR}^2}}}$$

which as we can see now has a dependence on both the IR and XUV duration τ_{IR} and τ_{XUV} (Figure 3b).

If we now fix the IR intensity and let τ_{IR} vary, we notice that the values calculated through SFA and this non-adiabatic model diverge at high intensities (Figure 4b). From this we deduce that the A_{IR}^2 term we previously neglected is instead relevant.

3.3. Addition of the quadratic term

If we put the quadratic term back in the phase of the spectrogram, through few calculations we obtain the new spectrogram

$$S(\omega,\tau) = \left| \int_{-\infty}^{+\infty} \mathbf{E}_{XUV}(t+\tau) e^{ip_C\frac{E_0(t)}{\omega_0^2}\sin(\omega_0 t)} \cdot \right.$$
$$\left. \cdot e^{i\frac{E_0^2(t)}{8\omega_0^3}\sin(2\omega_0 t)} e^{i\omega t} dt \right|^2$$

By applying again the Jacobi-Anger expansion on the two exponentials, we are able to write the integral as the Fourier transform of the product of two summations of Bessel functions. This product gives origin to a new function, often referred to as *generalised Bessel function*:

$$\mathcal{J}_n(u,v) = \sum_{m=-\infty}^{+\infty} J_n(u)\cdot J_m(v)$$

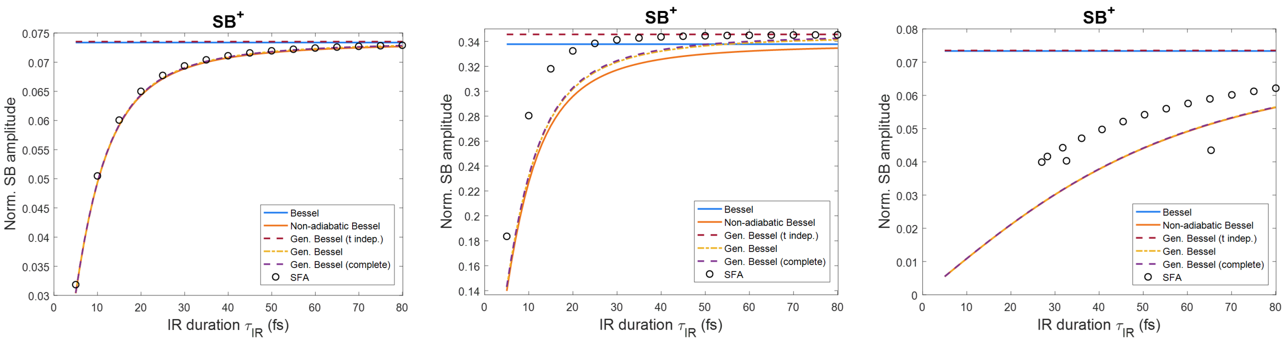

(a) (b) (c)

Figure 4: SB$^+$ amplitude as a function of τ_{IR} in $\tau = 0$. Here, $\tau_{XUV} = 11$ fs and (a) $I_{IR} = 10^{11} \frac{W}{cm^2}$, (b) $I_{IR} = 10^{12} \frac{W}{cm^2}$, (c) $I_{IR} = 10^{11} \frac{W}{cm^2}$ with dispersion.

where $u = -p_C \frac{E_0(t)}{\omega_0^2}$ and $v = -\frac{E_0^2(t)}{8\omega_0^3}$.
Hence, our new sideband amplitudes at $\tau = 0$ become

$$SB_0^{N\pm} = \left| \sum_{\substack{n=-\infty \\ n+2m=N}}^{+\infty} \mathcal{J}_n(u, v) \right|^2 \frac{1}{\sqrt{1 + |N| \frac{\tau_{XUV}^2}{\tau_{IR}^2}}}$$

This yields the results of Figure 3c.
Now let us compare the three models for SB$^+$ to the SFA simulations as a function of the IR duration with different IR intensities (Figure 4). For a short IR duration, the sideband amplitude decreases in both non-adiabatic Bessel and generalised Bessel models, and the latter is also closer to the actual SFA simulations. Though, the approximation of Eq. (4) becomes less reliable for $I_{IR} \geq 10^{12} \frac{W}{cm^2}$, and so do both models. For long IR pulses SFA simulations and generalised Bessel functions follow the same asymptote. Dispersion also heavily affects the results, rendering the model less effective for high values of GDD, TOD and FOD (Figure 4c).

4. Data analysis

We shall start by considering a long IR pulse ($\tau_{IR} \to +\infty$), and we let the IR intensity vary from $I_{IR} = 5 \cdot 10^{10} \frac{W}{cm^2}$ to $I_{IR} = 2 \cdot 10^{12} \frac{W}{cm^2}$. The experimental results follow the generalised Bessel shape, yet they are not superimposed with the theoretical lines. We can correct this discrepancy if we take into account the correction factors due to the lens and drift parameters of the ToF spectrometer. This way the data are in good agreement with the theoretical model (Figure 5). Hence, we deem our model **reliable** inside the explored range of intensities.
When investigating IR pulses of variable time duration ($\tau_{IR} = 5 \div 50$ fs) we fix the IR intensity at $I_{IR} = 5 \cdot 10^{11} \frac{W}{cm^2}$. From Figure 6 we observe that the overall trend of the data abides by the expected behaviour of the generalised Bessel model. Nevertheless, the final curve given by the data does not seem to be monotonic. This discrepancy is to be attributed to pulse dispersion. Through STRIPE reconstructions, which account for dispersion, we are able to replicate the behaviour of the data.

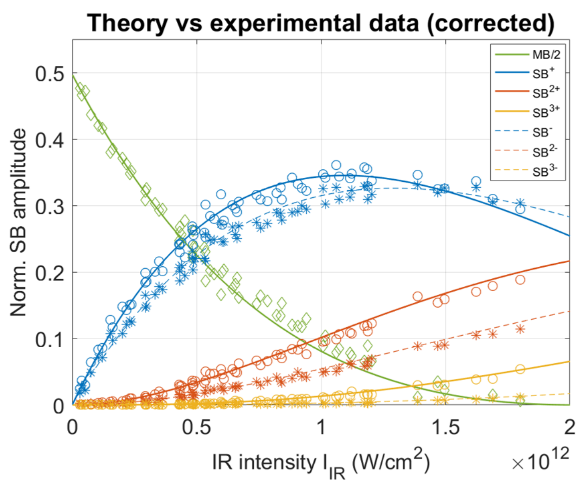

Figure 5: SB amplitudes (model and data) as a function of I_{IR}.

5. Conclusions

In this thesis we explored the limits of Floquet theory, which deals with periodic systems, by means of pulses with a reduced periodicity (few-cycle), both as a function of their intensity and

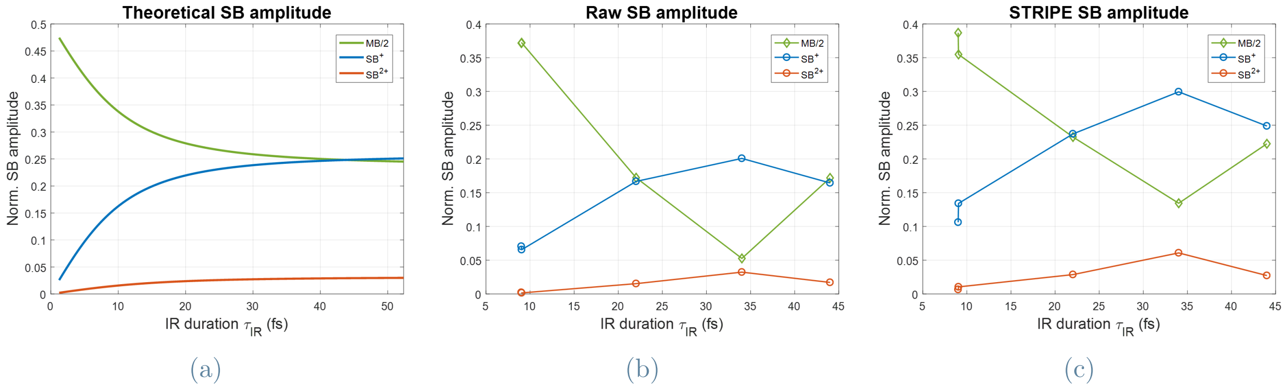

Figure 6: SB amplitudes as a function of τ_{IR} (a) found with the generalised Bessel model, (b) acquired experimentally and (c) reconstructed through STRIPE.

duration. We performed two-colour pump-probe experiments with few-femtosecond pulses on a Ne gas target. We employed XUV pulses to generate free electrons and populate the main band, the bare state of our system, and a series of IR pulses to generate the sidebands, i.e. the dressed states.

These experiments are described via the SFA model, from which we derived the generalised Bessel model after a series of calculations. This model correctly describes our phenomenon for long IR pulses, and for short IR pulses up to an intensity of $I_{IR} < 10^{12} \frac{W}{cm^2}$, provided both IR and XUV pulses are not affected by a large dispersion.

We compared this model to our data and found a good agreement in case of long IR pulses analysing the SB normalised amplitudes as a function of I_{IR}. Instead, when dealing with short IR pulses and studying bands amplitudes as a function of τ_{IR} for $I_{IR} = 5 \cdot 10^{11} \frac{W}{cm^2}$, we found the experimental data to qualitatively follow the model, predicting a SB amplitude that decreases with shorter pulses. The discrepancy between the experimental results and the model is attributed to the non-idealities of the IR pulses (fluctuations in intensity and wavelength, spectral chirp). In the future, we will use the STRIPE reconstructions to estimate the actual pulse parameters used in the experiment and correct the data for any non-ideality.

Nevertheless, already at this early stage, the results presented in this thesis show that the Floquet theory can be applied to the short-pulse limit, if the amplitude of the dressed states is opportunely rescaled. This finding, never observed before, will be of great interest for the development of Floquet engineering at the short time scales, moving an important step towards a complete optical control of new metastable exotic states of matter with ultrashort light pulses.

References

[1] Bruno Moio et al. Reconstruction of few-fs XUV pulses with a perturbative approach. *EPJ Web of Conferences*, 255:11008, 2021.

[2] Lukas Medišauskas, Ulf Saalmann, and Jan Rost. Floquet hamiltonian approach for dynamics in short and intense laser pulses. *Journal of Physics B: Atomic, Molecular and Optical Physics*, 52(1):015602, dec 2018.

[3] Peter Mulser and Dieter Bauer. *High Power Laser-Matter Interaction.* Springer Berlin Heidelberg, 2010.

[4] Takashi Oka and Sota Kitamura. Floquet engineering of quantum materials. *Annual Review of Condensed Matter Physics*, 2019.

[5] Luca Poletto and Paolo Villoresi. Time-delay compensated monochromator in the off-plane mount for extreme-ultraviolet ultrashort pulses. *Applied Optics*, 45(34):8577, December 2006.